OPEN

Quantification of Hepatic Fat Fraction in Patients With Nonalcoholic Fatty Liver Disease: Comparison of Multimaterial Decomposition Algorithm and Fat (Water)-Based Material Decomposition Algorithm Using Single-Source Dual-Energy Computed Tomography

Qinhe Zhang, MD, Ying Zhao, MD,* Jingjun Wu, MD,* Luhan Xie, MS,† Anliang Chen, MS,* Yijun Liu, MS,* Qingwei Song, MS,* Jianying Li, MD,‡ Tingfan Wu, MD,§ Lizhi Xie, MD,‡ and Ailian Liu, MD**

Objective: The purpose of this study was to evaluate the accuracy of quantifying hepatic fat fraction (HFF) in nonalcoholic fatty liver disease patients with multimaterial decomposition (MMD) and fat (water)-based material decomposition by single-source dual-energy computed tomography.

Methods: Hepatic fat fractions were quantified by noncontrast ($HFF_{non\text{-}CE}$) and contrast-enhanced single-source dual-energy computed tomography in arterial phase (HFF_{AP}), portal venous phase (HFF_{PVP}) and equilibrium phase (HFF_{EP}) using MMD in 19 nonalcoholic fatty liver disease patients. The fat concentration was measured on fat (water)-based images. As the standard of reference, magnetic resonance iterative decomposition of water and fat with echo asymmetry and least-squares estimation-iron quantification images were reconstructed to obtain HFF ($HFF_{IDEAL\text{-}IQ}$).

Results: There was a strong correlation between $HFF_{non\text{-}CE}$, HFF_{AP}, HFF_{PVP}, HFF_{EP}, fat concentration and $HFF_{IDEAL\text{-}IQ}$ ($r = 0.943$, 0.923, 0.942, 0.952, and 0.726) with HFFs having better correlation with $HFF_{IDEAL\text{-}IQ}$. Hepatic fat fractions did not significantly differ across scanning phases. The HFFs of 3-phase contrast-enhanced computed tomography had a good consistency with $HFF_{non\text{-}CE}$.

Conclusions: Hepatic fat fraction using MMD has excellent correlation with that of magnetic resonance imaging, is independent of the computed tomography scanning phases, and may be used as a routine technique for quantitative assessment of HFF.

Key Words: multimaterial decomposition, computed tomography, nonalcoholic fatty liver disease, quantitative, fat

(*J Comput Assist Tomogr* 2021;45: 12–17)

Nonalcoholic fatty liver disease (NAFLD) is the most common cause of chronic liver diseases in children and adolescents, and also the leading cause of liver diseases in adults.[1] Its worldwide prevalence is between 10% and 30%, whereas the prevalence in Asian countries is between 11% and 16% (~15% in China).[2,3] Nonalcoholic fatty liver disease is mainly caused by excessive accumulation of triacylglycerol in hepatic cells and is closely related to type 2 diabetes mellitus, hypertension, metabolic syndrome,[4] and increased risk of developing cardiovascular disease.[5] Nonalcoholic fatty liver disease is a reversible disease, which can be cured by early diagnosis and timely treatment. Nevertheless, if not appropriately treated, it can result in nonalcoholic steatosis, hepatitis, fibrosis, cirrhosis, and even hepatic cell cancer.[6] Some studies have shown that nonalcoholic fatty liver–related cirrhosis has a worse prognosis than hepatitis cirrhosis; 10% to 20% of patients with nonalcoholic fatty liver-related cirrhosis die from liver failure complications or require liver transplantation.[7–9] Therefore, the accurate evaluation of the liver fat content is very important for the early diagnosis and intervention of the disease. Biopsy is the criterion standard for assessing hepatic fat fraction (HFF), yet it is an invasive examination that is not well accepted by all patients. Therefore, precise and noninvasive imaging methods for the clinical evaluation of NAFLD are needed.

Magnetic resonance spectroscopy (MRS) is considered the most accurate noninvasive method for measuring and quantifying HFF.[10–12] However, this method requires long postprocessing time and patient's respiratory coordination, and is subject to sampling errors associated with a low spatial resolution.[13,14] Besides this, the HFF measured by MRS does not represent the whole liver. Recently, iterative decomposition of water and fat with echo asymmetry and least-squares estimation-iron quantification (IDEAL-IQ) sequence has been shown to have numerous advantages compared with MRS.[11,15,16] It can provide an accurate and reliable fat fraction of the whole liver by a single breath-hold scanning.[17,18]

In clinical practice, abdominal computed tomography (CT) has been a more convenient method than abdominal magnetic resonance imaging (MRI) for screening and early diagnosing of NAFLD. Traditional CT attenuation value is a convenient method for analyzing HFF, yet it is considered a semiquantitative approach that could be affected by variable tube voltage settings and iron overload.[19] Recently, an advanced tool based on multimaterial decomposition (MMD) algorithm has been developed to generate liver fat quantification (LFQ) maps to quantify HFF using a single-source dual-energy computed tomography (ssDECT).[20,21] Studies have shown that the fat concentration from the 2-material decomposition (MD) algorithm using the fat (water)-based material images has good agreements with histopathological results.[22,23] Because the MMD algorithm considers fat, liver tissue, and others, such as iron or iodinated contrast media in the liver, one study has shown that it has at least comparable sensitivity and specificity with

From the *Department of Radiology, The First Affiliated Hospital of Dalian Medical University; †Department of Biotechnology, Dalian Medical University, Dalian; ‡GE Healthcare, MR Research, Beijing; and §GE Healthcare (China), Translational Medicine Team, Shanghai, China.

Received for publication March 24, 2020; accepted September 10, 2020.

Correspondence to: Ailian Liu, MD, Department of Radiology, The First Affiliated Hospital of Dalian Medical University, Xigang District, Zhongshan Rd, No. 222, Dalian, China (e-mail: liuailian@dmu.edu.cn).

This study was supported by Program for Training Capital Science and Technology Leading Talents (Z181100006318003).

The authors declare no conflict of interest.

DOI: 10.1097/RCT.0000000000001112

TABLE 1. Patients' Characteristics

Characteristics	Value
Total no. patients	19
Male/female	11/8
Age, y	61.00 (57.50–68.00)
BMI, kg/m^2	26.33 (25.18–28.54)
Interval between CT and MRI scan, d	3.00 (2.50–5.00)

BMI indicates body mass index.

the CT attenuation value of the non–contrast-enhanced ssDECT for the detection of hepatic steatosis.[24] Nevertheless, so far, no studies have reported on the accuracy between LFQ maps and fat (water)-based images in NAFLD patients. Therefore, the purpose of our study was to evaluate the feasibility and accuracy of performing live fat quantification in NAFLD patients with HFF measurement on LFQ maps and fat concentration measurement on fat (water)-based images in ssDECT, while assessing the value of multiphasic CT for assessment of HFF and the consistency between in different CT phases, using the results obtained with MRI IDEAL-IQ sequence as a reference standard.

MATERIALS AND METHODS

Patients

This was a retrospective study, which was approved by the hospital ethical committee. A total of 47 patients between October 2017 and January 2019 were screened retrospectively for possible inclusion in our study. The inclusion criteria were the following: (1) patients diagnosed with NAFLD and (2) those who underwent ssDECT and MRI scanning (the interval between CT and MRI scanning was less than 15 days[20]). Exclusion criteria were as follows: (1) underwent a conventional CT scanning (n = 22), (2) no 3-phase contrast-enhanced scanning was applied (n = 1), (3) no IDEAL-IQ sequence (n = 3), and (4) poor image quality (poor signal-to-noise ratio or motion artifacts) (n = 2).

Finally, 19 patients were enrolled, including 11 men and 8 women (age range, 42–73 years [median, 61 years]; body mass index range, 19.33–37.86 kg/m^2 [median, 26.33 kg/m^2]). The patients' characteristics are summarized in Table 1.

Scanning Methods

ssDECT Scanning

All abdominal ssDECT scanning was performed on a Revolution CT scanner (GE Healthcare, Chicago, IL). Briefly, patients fasted for 4 to 6 hours. Before scanning, patients were placed in a supine position. Different gemstone spectral imaging (GSI) protocols were used for the non–contrast-enhanced phase and the 3 contrast-enhanced phases for each patient by using different tube currents in the protocol setting, and the 3 contrast-enhanced phases shared the same GSI protocol. The GSI protocol was also adjusted based on patient's body mass index. However, the tube current cannot be changed during the scan. The ssDECT scanning parameters were as follows: rapid switching between tube voltages of 80 kVp and 140 kVp, tube current of 230 to 445 mA, adaptive statistical iterative reconstruction-Veo of 40%, detector width of 80 mm, pitch of 0.992, tube rotation speed of 0.6 scan interval/rotation time, slice thickness of 1.25 mm, and slice interval of 1.25 mm. The non–contrast-enhanced abdominal scanning was acquired first. After the non–contrast-enhanced CT scanning, a high-pressure injector was used to administer the contrast agent iohexol (Omnipaque 300 mg/mL; GE Healthcare) at a dosage of 1.0 mL/kg body weight via the median cubital vein at a flow rate of 4 mL/s. Arterial-phase (AP), portal venous-phase (PVP), and equilibrium-phase (EP) contrast-enhanced images were obtained at 30, 60, and 120 seconds, respectively, after contrast agent injection. The ssDECT scans were performed at the end of inhalation, and scanning ranged from the dome of diaphragm to pubic symphysis.

MRI Scanning

Magnetic resonance imaging scanner (Signa, HDxt; GE Medical Systems, Inc., Waukesha, WI) with an 8-channel phased-array body coil was used. Briefly, patients fasted for 4 to 6 hours and were trained to exhale and hold their breath for more than 20 seconds before scanning. The subjects were examined in the supine position. A 3-plane localization imaging gradient-echo sequence was performed at the beginning of acquisition. Parameters of the IDEAL-IQ sequence were as follows: repetition time/echo time, 13.4 milliseconds/4.8 milliseconds; slice thickness, 10 mm; bandwidth, 125 kHz; field of view, 36 cm × 36 cm; matrix, 256 × 160; flip angle, 5 degrees; number of excitation, 1; and breath-hold scanning. The images were processed using IDEAL Research software provided by the manufacturer to generate water, fat, in phase, out phase, R2*, and fat fraction image.

Image Generation and Analysis

MRI Image Generation and Analysis

The IDEAL-IQ fat fraction images were uploaded to an Advantage Workstation 4.7 (AW4.7; GE Healthcare). Images were measured and analyzed by 2 experienced radiologists (observer 1 and observer 2, with 6 and 10 years of experience in abdominal MRI imaging, respectively). One 2-dimensional region of interest (ROI; size, the diameter of 30 mm) was placed in the right lobe of the liver in the IDEAL-IQ fat fraction images while carefully avoiding large vessels, bile ducts, and lesions. The HFF of IDEAL-IQ ($HFF_{IDEAL-IQ}$) was automatically calculated (Fig. 1).

ssDECT Image Generation and Analysis

After the ssDECT scanning, all images were transferred to an Advanced Workstation 4.7 (AW4.7; GE Healthcare), and 2 types of ssDECT images were reconstructed at 5.0-mm image slice

FIGURE 1. One 2D ROI was placed in the right lobe of the liver in the IDEAL-IQ fat fraction image while carefully avoiding large vessels, bile ducts, and lesions. 2D, 2-dimensional.

thickness and image interval using GSI software: fat (water)-based images in non–contrast-enhanced phase and LFQ maps in AP, PVP, and EP. To measure $HFF_{non\text{-}CE}$, HFF_{AP}, HFF_{PVP}, and HFF_{EP}, one 2-dimensional ROI (size, the diameter of 30 mm) was placed in LFQ maps in the non–contrast-enhanced phase, in the same position as the IDEAL-IQ fat fraction images. Similar image slices were selected manually among different imaging phases to offset potential breathing-induced anatomy shift for generating LFQ maps, and copy function (on AW) was used to place ROI at the same location on the right liver lobe for all phases in each patient (Fig. 2) by 2 experienced radiologists (observer 1 and observer 2, with 6 and 10 years of experience in abdominal CT imaging, respectively; both were blinded to the results of IDEAL-IQ). On fat (water)-based images in the non–contrast-enhanced phase, fat concentration was measured at the same site in the same manner (Fig. 3). The volumetric CT dose index ($CTDI_{vol}$) and dose-length product reported by the CT scanner were recorded.

Statistical Analysis

All data were analyzed using SPSS version 25.0 (SPSS Inc., Chicago, IL). The normality of the variables was tested by the Shapiro-Wilk test. Normally distributed data were expressed as means ± SDs, and nonnormally distributed data were expressed as medians and ranges (25th, 75th percentiles). The intraclass correlation coefficient (ICC) was used to check the consistency of the 2 observers: ICC value of <0.4 indicated poor consistency, whereas ICC value of >0.80 indicated good consistency; if the consistency was good, the average data were selected for subsequent analysis. When parameters were normally distributed, the Pearson correlation coefficient was used; otherwise, the Spearman correlation coefficient was used. Correlation coefficients were interpreted as follows: weak, 0 to 0.4; moderate, 0.4 to 0.7; and strong, 0.7 to 1.0. The HFFs of the 3 contrast-enhanced phases were compared with $HFF_{non\text{-}CE}$ to determine the reproducibility of the MMD algorithm by using ICC and Kruskal-Wallis test or analysis of variance test for normally or abnormally distributed data, respectively. A 2-tailed P value of <0.05 was considered to be statistically significant.

FIGURE 3. In fat (water)-based images in non–contrast-enhanced phase, fat concentration was measured by placing one 2D ROI, as the same position as the ROI in IDEAL-IQ fat traction images. 2D, 2-dimensional.

RESULTS

Consistency Analysis

Two observers measured all data. The data consistency is shown in Table 2. The ICC was greater than 0.80, which suggested good agreement. Average data were selected for subsequent analysis.

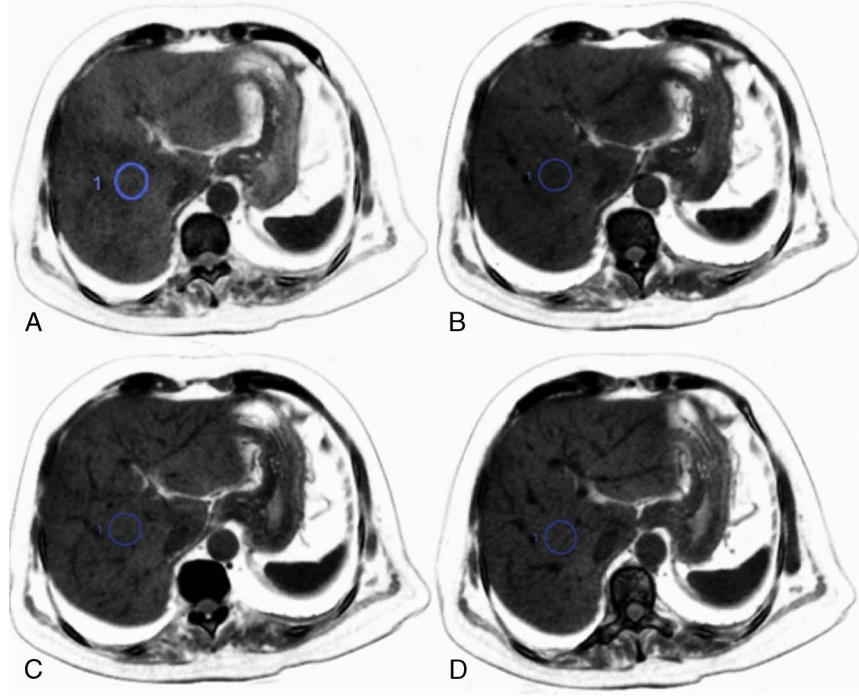

FIGURE 2. One 2D ROI was placed in LFQ maps in non–contrast-enhanced phase (A), in the same position as the IDEAL-IQ fat fraction images, and the copy function was used to determine LFQ maps at the same ROI location for AP, PVP, and EP (B–D). 2D, 2-dimensional.

TABLE 2. Two-Observer Measurements of the Consistency

Parameters	Observer 1	Observer 2	ICC Value
$HFF_{IDEAL-IQ}$, %	12.20 (8.20–13.20)	12.02 ± 4.94	0.972
HFF_{non-CE}, %	11.45 ± 4.07	11.12 ± 3.93	0.964
HFF_{AP}, %	10.76 (9.79–12.46)	11.41 ± 4.10	0.963
HFF_{PVP}, %	11.70 ± 4.15	11.83 ± 4.29	0.976
HFF_{EP}, %	11.55 ± 4.52	11.14 ± 4.94	0.976
Fat concentration, mg/cm^3	−100.64 ± 62.45	−101.99 ± 64.32	0.998

Correlation Analysis

As shown in Figures 4 and 5, there was a strong correlation between HFF_{non-CE}, HFF_{AP}, HFF_{PVP}, HFF_{EP}, fat concentration (measured in the non–contrast-enhanced phase), and $HFF_{IDEAL-IQ}$ ($r = 0.943$, 0.923, 0.942, 0.952, and 0.726; $P < 0.05$). The detailed HFF_{non-CE}, HFF_{AP}, HFF_{PVP}, HFF_{EP}, fat concentration, and $HFF_{IDEAL-IQ}$ are shown in Table 3.

Difference and Consistency Analysis of HFF in All Phases

As shown in Figure 6, there were no significant differences in HFFs in all phases ($P > 0.05$). Besides this, the HFF of 3-phase had good consistency with HFF_{non-CE} (ICC, 0.985, 0.976, and 0.912).

Patient Radiation Dose

The mean ± SD $CTDI_{vol}$ (mGy) in non–contrast-enhanced and contrast-enhanced phase were 11.17 ± 1.06 and 10.36 ± 1.59, respectively. The mean ± SD dose-length product (mGy-cm) in the non–contrast-enhanced phase, AP, PVP, and EP was 520.45 ± 151.00, 474.96 ± 152.35, 474.99 ± 152.33, and 474.89 ± 152.45, respectively.

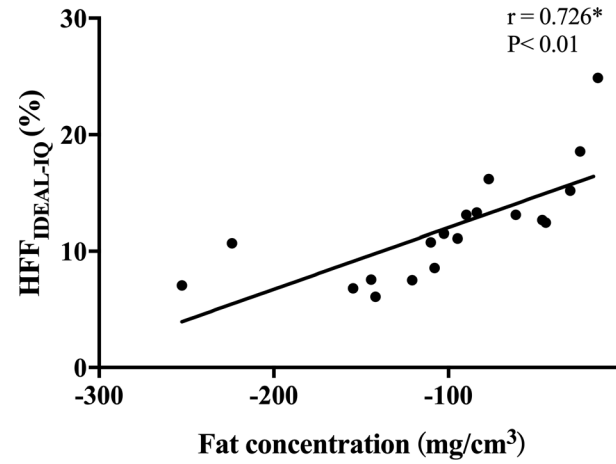

FIGURE 5. Correlation between fat concentration and $HFF_{IDEAL-IQ}$. *Pearson's correlation coefficient.

DISCUSSION

The results of our study showed that IDEAL-IQ, HFF measurements on LFQ maps, and fat concentration measurement on fat (water)-based MD images all had good reproducibility for quantitative measurement of liver fat. Although the HFF values of LFQ maps in all phases and fat concentration were all strongly correlated with those of IDEAL-IQ, HFFs had much stronger correlation. Furthermore, the HFFs from the 3 contrast-enhanced phases were consistent with that from the non–contrast-enhanced phase (HFF_{non-CE}).

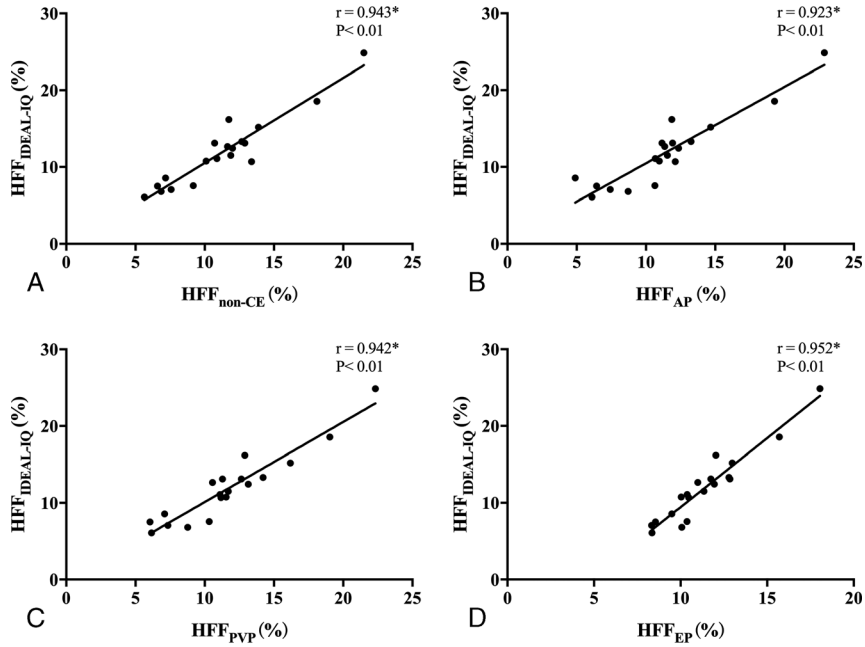

FIGURE 4. A, Correlation between HFF_{non-CE} and $HFF_{IDEAL-IQ}$. B, Correlation between HFF_{AP} and $HFF_{IDEAL-IQ}$. C, Correlation between HFF_{PVP} and $HFF_{IDEAL-IQ}$. D, Correlation between HFF_{EP} and $HFF_{IDEAL-IQ}$. *Pearson's correlation coefficient. Non-CE indicates non–contrast-enhanced; AP, arterial phase; PVP, portal venous phase; EP, equilibrium phase.

TABLE 3. $HFF_{IDEAL-IQ}$, HFF_{non-CE}, HFF_{AP}, HFF_{PVP}, HFF_{EP}, and Fat Concentration for NAFLD Patients

Parameters	Value
$HFF_{IDEAL-IQ}$, %	11.95 ± 4.61
HFF_{non-CE}, %	11.29 ± 3.93
HFF_{AP}, %	11.49 ± 4.28
HFF_{PVP}, %	11.76 ± 4.17
HFF_{EP}, %	11.40 ± 2.44
Fat concentration, mg/cm^3	−101.32 ± 63.34

Liver biopsy is still considered the criterion standard for calculating the liver fat content. Nevertheless, it can also result in sample errors and poor repeatability, as well as cause bleeding, bile leakage, and other complications.[25,26] For these reasons, noninvasive imaging techniques, such as ultrasound, MRI, and ssDECT, have been applied to quantitatively assess liver fat content quantitatively in clinic or research. For example, ultrasound is a widely recognized imaging approach that has a low cost and does not produce radiation. However, its major limitations are the operation dependence and poor objectivity, making the positive predictive value of ultrasound for fatty liver only 34.5%.[27]

Iterative decomposition of water and fat with echo asymmetry and least-squares estimation-iron quantification based on MRI is considered the best noninvasive technique for assessing liver fat content. It uses a 6-echo 3-point Dixon method to minimize T2* interference and reduces the effects of fat peak multiplicity, signal-to-noise ratio deviation, and eddy currents on the results, thus making proton density in tissues the main factor affecting signal intensity. By using IDEAL-IQ, HFF can be automatically obtained without postprocessing or calculation.[28] A recent meta-analysis study confirmed that IDEAL-IQ was extremely reproducible and accurate in assessing liver fat content, regardless of field strengths.[29] Iterative decomposition of water and fat with echo asymmetry and least-squares estimation-iron quantification can be used to obtain proton density fat fraction, which is correlated but not equivalent to real mass fat fraction.[30] In this study, IDEAL-IQ was used as a reference technique to examine the feasibility and accuracy of quantifying liver fat in NAFLD patients using HFF by MMD algorithm and fat concentration by MD algorithm in ssDECT.

Computed tomography attenuation value can be used to evaluate the liver fat content using ssDECT. Measurements of CT attenuation can assess liver fat content according to the inverse relationship between liver fat content and liver CT attenuation.[31] Because the presence of contrast media can skew measurements of liver CT attenuation, this method can only be applied in a non–contrast-enhanced phase.[31,32] In addition, evaluation of liver fat content could be affected by iron, gold, manganese, and other heavy metal deposition in the liver and spleen or the administration of amiodarone and other drugs.[33–36] Previous studies revealed that average liver CT attenuation normalized by the spleen, and either involving calculating differences (liver minus spleen) or ratios (usually, spleen to the liver), showed a high correlation with pathological results and could be used to assess the liver fat content.[34,37,38] Importantly, CT indices that use liver and spleen attenuations have been shown to have a better metric compared with liver attenuation alone.[37] However, it can only perform semiquantitative analysis of liver fat and cannot obtain accurate liver fat content.[39]

Using fat (water)-based image by ssDECT is another method for quantitative assessment of the fat deposition in the liver. Previous studies have shown that fat concentration obtained from the MD images had a good correlation with a fat percentage from the pathological analysis in rats.[22,40] Although it is a quantitative analysis of liver fat content, it cannot directly produce intuitive percentage of fat because MD images use fat and water as the basis material pair to measure the fat concentration, thus reflecting the changes in fat concentration rather than a fat percentage. However, in our study, we did find that there was a strong correlation between fat concentration and $HFF_{IDEAL-IQ}$.

As a novel method with ssDECT to assess liver fat content, MMD has 2 main implications for patient care. It adds a quantitative and intuitive assessment of liver fat content for LFQ maps.[20] It is based on the volume conservation,[41] and the fat volume fraction can be automatically calculated. Our results demonstrated that, compared with the IDEAL-IQ technology, HFFs calculated by MMD in each phase of ssDECT had a very strong correlation with $HFF_{IDEAL-IQ}$. Moreover, its relevance was significantly higher than that of fat (water) concentration. These increased the clinical application of ssDECT in NAFLD. On the other hand, MMD is a potential technique for decreasing radiation dose. This is because fat, liver tissue, and blood are used as the material basis in MMD, and iodine contrast agents are also considered by applying the virtual unenhancement image in the case of contrast-enhanced ssDECT images when HFF calculation is performed.[21,42] In this way, HFF can be measured from the contrast-enhanced scanning; thus, the need for non–contrast-enhanced scanning may be eliminated in some patients.[20,24] Our experimental results verified this conclusion.

This study had several limitations. First, the sample size was small. This is because we strictly controlled the time interval between ssDECT and MRI scans to prevent changes in liver fat content. In addition, we used IDEAL-IQ based on MRI as a reference rather than a liver biopsy. Finally, we only placed 1 ROI in the right lobe of the liver; because the purpose of the study was to assess the accuracy of MMD algorithm and fat (water)-based MD algorithm, we tried to ensure that all ROIs were at the same level.

CONCLUSIONS

The quantification of liver fat content using HFF measurement on LFQ maps and fat concentration measurement on fat (water)-based images are all well correlated with that of MR IDEAL-IQ images. Compared with fat (water)-based images, the quantification of liver fat content using LFQ maps has stronger correlation with MRI measurement and more intuitive, and thus could be used as a routine technique for quantitative assessment of hepatic fat content.

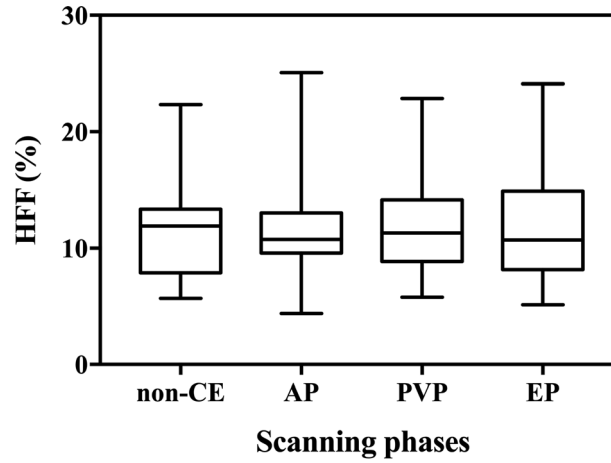

FIGURE 6. Hepatic fat fractions did not significantly differ across scanning phases ($P > 0.05$).

REFERENCES

1. Della Corte C, Mosca A, Majo F, et al. Nonalcoholic fatty pancreas disease and nonalcoholic fatty liver disease: more than ectopic fat. *Clin Endocrinol (Oxf)*. 2015;83:656–662.
2. Farrell GC, Wong VW, Chitturi S. NAFLD in Asia—as common and important as in the West. *Nat Rev Gastroenterol Hepatol*. 2013;10:307–318.
3. Forbes S, Taylor-Robinson SD, Patel N, et al. Increased prevalence of non-alcoholic fatty liver disease in European women with a history of gestational diabetes. *Diabetologia*. 2011;54:641–647.
4. Graffy PM, Pickhardt PJ. Quantification of hepatic and visceral fat by CT and MR imaging: relevance to the obesity epidemic, metabolic syndrome and NAFLD. *Br J Radiol*. 2016;89:20151024.
5. Adams LA, Anstee QM, Tilg H, et al. Non-alcoholic fatty liver disease and its relationship with cardiovascular disease and other extrahepatic diseases. *Gut*. 2017;66:1138–1153.
6. Lewis JR, Mohanty SR. Nonalcoholic fatty liver disease: a review and update. *Dig Dis Sci*. 2010;55:560–578.
7. Doycheva I, Issa D, Watt KD, et al. Nonalcoholic steatohepatitis is the most rapidly increasing indication for liver transplantation in young adults in the United States. *J Clin Gastroenterol*. 2018;52:339–346.
8. Bhala N, Angulo P, van der Poorten D, et al. The natural history of nonalcoholic fatty liver disease with advanced fibrosis or cirrhosis: an international collaborative study. *Hepatology*. 2011;54:1208–1216.
9. Charlton MR, Burns JM, Pedersen RA, et al. Frequency and outcomes of liver transplantation for nonalcoholic steatohepatitis in the United States. *Gastroenterology*. 2011;141:1249–1253.
10. Kang BK, Kim M, Song SY, et al. Feasibility of modified Dixon MRI techniques for hepatic fat quantification in hepatic disorders: validation with MRS and histology. *Br J Radiol*. 2018;91:20170378.
11. Grimm A, Meyer H, Nickel MD, et al. Repeatability of Dixon magnetic resonance imaging and magnetic resonance spectroscopy for quantitative muscle fat assessments in the thigh. *J Cachexia Sarcopenia Muscle*. 2018; 9:1093–1100.
12. Haufe WM, Wolfson T, Hooker CA, et al. Accuracy of PDFF estimation by magnitude-based and complex-based MRI in children with MR spectroscopy as a reference. *J Magn Reson Imaging*. 2017;46:1641–1647.
13. Springer F, Machann J, Claussen CD, et al. Liver fat content determined by magnetic resonance imaging and spectroscopy. *World J Gastroenterol*. 2010;16:1560–1566.
14. Li G, Xu Z, Gu H, et al. Comparison of chemical shift-encoded water-fat MRI and MR spectroscopy in quantification of marrow fat in postmenopausal females. *J Magn Reson Imaging*. 2017;45:66–73.
15. Kinner S, Reeder SB, Yokoo T. Quantitative imaging biomarkers of NAFLD. *Dig Dis Sci*. 2016;61:1337–1347.
16. Reeder SB, Cruite I, Hamilton G, et al. Quantitative assessment of liver fat with magnetic resonance imaging and spectroscopy. *J Magn Reson Imaging*. 2011;34:729–749.
17. Chen Y, Jiang Z, Long L, et al. Magnetic resonance imaging: proton density fat fraction for assessment of pancreatic fatty infiltration during progression of T2DM bama minipigs. *J Magn Reson Imaging*. 2019;50: 1905–1913.
18. Wang Q, Ye F, Ma P, et al. Quantitative magnetic resonance imaging evaluation of hepatic fat content with iron deposition: will it be disturbed? *J Int Med Res*. 2019;47:1958–1974.
19. Pickhardt PJ, Graffy PM, Reeder SB, et al. Quantification of liver fat content with unenhanced MDCT: phantom and clinical correlation with MRI proton density fat fraction. *AJR Am J Roentgenol*. 2018;211: W151–W157.
20. Hyodo T, Yada N, Hori M, et al. Multimaterial decomposition algorithm for the quantification of liver fat content by using fast-kilovolt-peak switching dual-energy CT: clinical evaluation. *Radiology*. 2017;283:108–118.
21. Mendonca PR, Lamb P, Sahani DV. A flexible method for multi-material decomposition of dual-energy CT images. *IEEE Trans Med Imaging*. 2014; 33:99–116.
22. Cao Q, Shang S, Han X, et al. Evaluation on heterogeneity of fatty liver in rats: a multiparameter quantitative analysis by dual energy CT. *Acad Radiol*. 2019;26:e47–e55.
23. Artz NS, Hines CD, Brunner ST, et al. Quantification of hepatic steatosis with dual-energy computed tomography: comparison with tissue reference standards and quantitative magnetic resonance imaging in the ob/ob mouse. *Invest Radiol*. 2012;47:603–610.
24. Hur BY, Lee JM, Hyunsik W, et al. Quantification of the fat fraction in the liver using dual-energy computed tomography and multimaterial decomposition. *J Comput Assist Tomogr*. 2014;38:845–852.
25. Kleiner DE, Brunt EM, Van Natta M, et al. Design and validation of a histological scoring system for nonalcoholic fatty liver disease. *Hepatology*. 2005;41:1313–1321.
26. Fassio E, Alvarez E, Domínguez N, et al. Natural history of nonalcoholic steatohepatitis: a longitudinal study of repeat liver biopsies. *Hepatology*. 2004;40:820–826.
27. Hernaez R, Lazo M, Bonekamp S, et al. Diagnostic accuracy and reliability of ultrasonography for the detection of fatty liver: a meta-analysis. *Hepatology*. 2011;54:1082–1090.
28. Idilman IS, Tuzun A, Savas B, et al. Quantification of liver, pancreas, kidney, and vertebral body MRI-PDFF in non-alcoholic fatty liver disease. *Abdom Imaging*. 2015;40:512–519.
29. Yokoo T, Serai SD, Pirasteh A, et al. Linearity, bias, and precision of hepatic proton density fat fraction measurements by using MR imaging: a meta-analysis. *Radiology*. 2018;286:486–498.
30. Hu HH, Börnert P, Hernando D, et al. ISMRM workshop on fat-water separation: insights, applications and progress in MRI. *Magn Reson Med*. 2012;68:378–388.
31. Kodama Y, Ng CS, Wu TT, et al. Comparison of CT methods for determining the fat content of the liver. *AJR Am J Roentgenol*. 2007;188:1307–1312.
32. Schwenzer NF, Springer F, Schraml C, et al. Non-invasive assessment and quantification of liver steatosis by ultrasound, computed tomography and magnetic resonance. *J Hepatol*. 2009;51:433–445.
33. Piekarski J, Goldberg HI, Royal SA, et al. Difference between liver and spleen CT numbers in the normal adult: its usefulness in predicting the presence of diffuse liver disease. *Radiology*. 1980;137:727–729.
34. Park SH, Kim PN, Kim KW, et al. Macrovesicular hepatic steatosis in living liver donors: use of CT for quantitative and qualitative assessment. *Radiology*. 2006;239:105–112.
35. Saadeh S, Younossi ZM, Remer EM, et al. The utility of radiological imaging in nonalcoholic fatty liver disease. *Gastroenterology*. 2002;123:745–750.
36. Zinreich SJ, Kennedy DW, Malat J, et al. Fungal sinusitis: diagnosis with CT and MR imaging. *Radiology*. 1988;169:439–444.
37. Byun J, Lee SS, Sung YS, et al. CT indices for the diagnosis of hepatic steatosis using non-enhanced CT images: development and validation of diagnostic cut-off values in a large cohort with pathological reference standard. *Eur Radiol*. 2019;29:4427–4435.
38. Yamada A, Sato KK, Kinuhata S, et al. Association of visceral fat and liver fat with hyperuricemia. *Arthritis Care Res*. 2016;68:553–561.
39. Sanyal AJ. AGA technical review on nonalcoholic fatty liver disease. *Gastroenterology*. 2002;123:1705–1725.
40. Sun T, Lin X, Chen K. Evaluation of hepatic steatosis using dual-energy CT with MR comparison. *Front Biosci (Landmark Ed)*. 2014;19:1377–1385.
41. Liu X, Yu L, Primak AN, et al. Quantitative imaging of element composition and mass fraction using dual-energy CT: three-material decomposition. *Med Phys*. 2009;36:1602–1609.
42. Fischer MA, Gnannt R, Raptis D, et al. Quantification of liver fat in the presence of iron and iodine: an ex-vivo dual-energy CT study. *Invest Radiol*. 2011;46:351–358.